

# A Leading Angle Flux Weakening Control Method for PMSM Based on Active Disturbance Rejection Control

Yanfei Pan, Xin Liu, Yilin Zhu\*, and Zhongshu Li

**Abstract**—A flux weakening (FW) control method of leading angle for a permanent magnet synchronous motor (PMSM) based on active disturbance rejection control (ADRC) is proposed to solve the problem of large fluctuation of speed, current, and torque in the control process. Firstly, according to the mathematical model of PMSM and its voltage and current constraints, the leading angle FW control algorithm is introduced. Then, according to the ADRC theory and the mathematical model of PMSM, the speed loop ADRC and current loop ADRC are constructed. The controller parameters are combined with the control bandwidth, and the parameter variation ranges are obtained by analyzing the stability of the control system. Finally, the proposed ADRC methods are combined with the leading angle FW control method to realize the ADRC leading angle FW control for PMSM, and the proposed method is verified on the experimental platform. The experimental results show that the proposed method has less speed, current, and torque fluctuations than the proportional integral (PI) controller method, which can effectively improve the motor control performance. At the same time, the controller parameters are combined with the bandwidth, which is convenient for practical engineering application.

## 1. INTRODUCTION

Permanent magnet synchronous motor (PMSM) is widely used in electric vehicles, wind power generation, computer numerical control (CNC) machine tools, and other fields due to its advantages of high efficiency, high power density, and easy flux weakening expansion. Electric vehicle system requires a wide speed regulation range to meet the requirements of high-speed driving, so the research on PMSM high-speed flux weakening control is very important. In the traditional flux weakening strategy, there are two current regulators and one speed regulator in the system, which adjust the  $d$ - $q$  axis currents and speed, respectively. The saturation of the regulators and the mutual coupling of the  $d$ - $q$  axis currents in the high-speed stage will deteriorate the regulation performance of the system to the motor speed, current, and torque, and even lead to system instability. Therefore, high-performance control of the PMSM flux weakening region is required [1, 2].

For FW control of a PMSM system, many scholars have put forward different control schemes and improvement methods. In [3], a voltage closed-loop is used to adjust the current angle value to realize the FW control of the interior PMSM. In [4], the voltage closed-loop is also used to realize the FW control. Different from [3], in this article, the FW control is realized by adjusting the  $d$ -axis current. At the same time, only one current regulator is used to adjust the  $d$ - $q$  axis currents. In [5], voltage closed-loop mode is used to adjust the  $d$ -axis current, and a six step over modulation strategy is adopted to improve the DC voltage utilization in the whole speed range. In [6], the voltage closed-loop control is used to adjust the angle to realize FW control, and the vector current regulator with anti-saturation is used to realize current regulation. In addition, the over modulation algorithm is combined with the proposed FW control to improve the control effect. In [7], Taylor series method is used to simplify

---

*Received 16 May 2022, Accepted 6 June 2022, Scheduled 22 June 2022*

\* Corresponding author: Yilin Zhu (yl.zhu.dy@gmail.com).

The authors are with the Jiangsu Changjiang Intelligent Manufacturing Research Institute Co, Ltd, Changzhou 213001, China.

the current distribution expression, and voltage closed-loop is used to realize the regulation function of  $d$ -axis current. However, the neglect operation of the higher-order term in Taylor series in this literature is not in place. If the coefficient of the higher-order term accounts for a large proportion, it will be inappropriate to continue to ignore it at this time. Therefore, the current distribution in this method cannot be applied to motors with different parameters. In [8], DC bus voltage disturbance is compensated, which almost achieves the maximum DC bus voltage utilization and improves the FW control performance. In [9], the leading angle FW control method is introduced, and the current distribution expressions corresponding to the leading angle are derived. Through these expressions, the current distribution is realized. In [10], the current controller based on feedback linearization algorithm is combined with the leading angle FW control algorithm to improve the control effect. In [11], the control based on robust second-order current and the hybrid FW control based on look-up table/voltage constraint tracking are combined to improve the effect of FW control. At the same time, the parameters such as inductance and flux linkage are estimated to improve the performance of robust second-order current controller. In [12], voltage phase is used to realize FW control. This method realizes FW control by reasonably distributing voltage, which is different from the way of distributing current. In the actual process of FW control, the current may not be optimally distributed. In [13], an improved single current regulator control scheme is proposed, which effectively improves the FW speed regulation range of the motor. This method has better applicability to motors with characteristic current less than rated current. The researches of FW control are not only in traditional vector control algorithm, but also in model-based predictive control. In [14], maximum torque per ampere (MTPA) control is used to distribute current in the constant torque area. When the speed exceeds the base speed, the motor will run in the FW control area and distribute the current using the theoretical formula. This method has the problem of poor robustness and poor effect in practical application. In [15], the set speed is also used as the switching point of FW control, which has poor effect in practical application.

The above FW control methods are generally realized by PI controller in the regulation process of speed and current. Because the design parameters of PI controllers are affected by bandwidth, a set of parameters cannot be applied to different speeds. In FW control, the speed range changes greatly, and the same group of PI control parameters will not be applicable to different speed ranges, while multiple groups of PI parameters are bound to complicate the parameter adjustment process. In order to improve the control performance of speed, current, and torque in the process of FW control, an active disturbance rejection leading angle FW control algorithm is proposed. In this algorithm, an active disturbance rejection controller (ADRC) with strong parameter robustness is used to replace the PI controller. By designing the parameters of the ADRC, the whole control system has strong steady-state control accuracy on the premise of meeting the control performance. At the same time, the speed and currents can be adjusted by designing different observer bandwidths. Then the speed loop ADRC, current loop ADRC, and lead angle FW control are combined to realize high-performance FW control. Finally, the effectiveness and correctness of the proposed algorithm are verified on the experimental platform. The experimental results show that the proposed method can significantly improve the control effect of motor speed, current, and torque, and has a good inhibitory effect on the fluctuation of speed, current, and torque during steady-state operation.

## 2. MATHEMATICAL MODEL OF PMSM

The stator voltage formulas of PMSM in a  $d$ - $q$  coordinate system can be expressed as

$$\begin{cases} u_d = Ri_d + L_d \frac{di_d}{dt} - \omega_e L_q i_q \\ u_q = Ri_q + L_q \frac{di_q}{dt} + \omega_e L_d i_d + \omega_e \lambda_f \end{cases} \quad (1)$$

where  $i_d$  and  $i_q$  are  $d$ - $q$  axis stator currents, respectively;  $R$  is the stator resistance;  $\lambda_f$  is the flux linkage of permanent magnet;  $\omega_e$  is the rotor electric angular velocity;  $L_d$  and  $L_q$  are  $d$ - $q$  axis stator inductances, respectively;  $L_d = L_q = L_s$  in a surface mounted PMSM,  $u_d$  and  $u_q$  are  $d$ - $q$  axis stator voltages, respectively.

When the motor is running at high-speed FW area, the voltage drop generated by the stator resistance part is far less than the back electromotive force (EMF) part; therefore, it can be ignored.

(1) can be simplified to

$$\begin{cases} u_d = -\omega_e L_q i_q \\ u_q = \omega_e (L_d i_d + \lambda_f) \end{cases} \quad (2)$$

In the control system, the power supply voltage has been determined, so there is a limit value for the voltage that the inverter can output. Define this maximum as  $U_{\max}$ , the voltage expressions satisfy

$$u_s^2 = u_d^2 + u_q^2 \leq U_{\max}^2 \quad (3)$$

where  $u_s$  is the stator voltage.

Current vector  $i_s$  is also limited, defining the maximum value of stator current as  $I_{\max}$ , and current meets

$$i_s^2 = i_d^2 + i_q^2 \leq I_{\max}^2 \quad (4)$$

### 3. LEADING ANGLE FW CONTROL ALGORITHM BASED ON ADRC

During the operation of PMSM, with the increase of rotating speed, the back EMF generated by PMSM is also gradually increasing. When the output voltage of the inverter reaches the limit, the speed of the motor will not continue to increase without special methods. Since the back EMF of the motor is related to the product of the motor speed and the air gap flux, the air gap flux must be weakened in order to continue to increase the speed.

#### 3.1. Principle of Leading Angle FW Control

In the  $d$ - $q$  axis coordinate system, the electrical angle of the stator current vector  $i_s$  ahead of the  $q$ -axis is defined as the current leading angle, which is recorded as  $\gamma$ , as shown in Fig. 1. Due to the limitation of inverter capacity, the voltage vector of PMSM during stable operation meets (3). After neglecting the stator voltage drop, substitute (2) into (3) to obtain the expression

$$(L_q i_q)^2 + (L_d i_d + \lambda_f)^2 \leq \frac{U_{\max}^2}{\omega_e^2} \quad (5)$$

According to (4) and (5), the voltage and current trajectory curves shown in Fig. 1 can be drawn. Because the inductances of  $d$ - $q$  axis are equal, the voltage trajectory corresponding to (5) is circular.

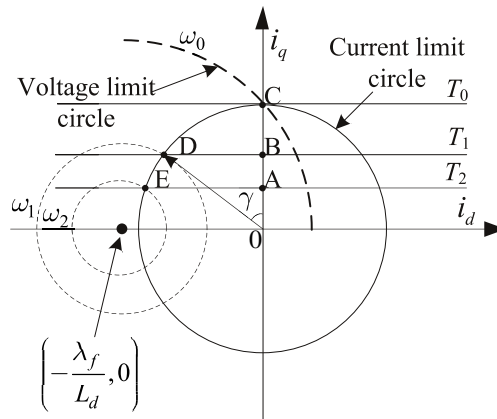


**Figure 1.** Voltage, current limit circle and current leading angle.

Based on the parameters of the prototype, the voltage-current limit trajectory curve is plotted as shown in Fig. 1. As the theoretical calculated value of the characteristic current point is located outside the current limit circle, only this case is analyzed. The FW process of the PMSM can be analyzed by means of Fig. 1. At speeds below the base speed, a vector control strategy with  $i_d = 0$  is used, and the stator current  $i_s$  is all used to generate the  $q$ -axis stator current  $i_q$ , when the leading angle  $\gamma = 0$ , and if

the load torque is  $T_2$ , the current trajectory is  $0 \rightarrow A$ . When the speed exceeds the turning speed, the inverter output capacity has reached the maximum value and cannot continue to provide the voltage required for the speed increase. At this time, the speed can only be increased by means of FW, i.e., increasing the  $d$ -axis current component  $i_d$  in the negative direction to weaken the amplitude of air gap flux linkage, at which time the leading angle  $\gamma$  starts to gradually increase; the speed reaches  $\omega_2$ ; and the current trajectory is  $A \rightarrow E$ . Similarly, when the load torque is  $T_1$  ( $T_1 > T_2$ ), the speed is stabilized to  $\omega_1$ , and the whole current trajectory is  $0 \rightarrow B \rightarrow C$ . When the load torque is  $T_0$  ( $T_0 > T_1 > T_2$ ), in order to increase the speed to  $\omega_1$ , the whole current trajectory is  $0 \rightarrow C \rightarrow D$ . When the motor is at point C, the motor runs steadily with torque  $T_0$  and speed  $\omega_0$ . After continuing to increase the speed to  $\omega_1$ , the torque decreases from  $T_0$  to  $T_1$ . FW also reduces the  $q$ -axis current component  $i_q$  to maintain the voltage balance, thus increasing the motor speed and achieving the purpose of FW to increase the speed.

### 3.2. Design of Active Disturbance Rejection Controller

A concise structure diagram of ADRC is shown in Fig. 2. By reasonably configuring the parameters of the extended state observer (ESO), the controlled object and ESO can be simplified into an integral series system. At this time, only the state error feedback (SEF) needs to be designed accordingly, so that the system can have better control effect. The tracking differentiator (TD) in Fig. 2 has the function of softening the input signal. Whether to use it can be determined according to the actual control situation [16, 17].

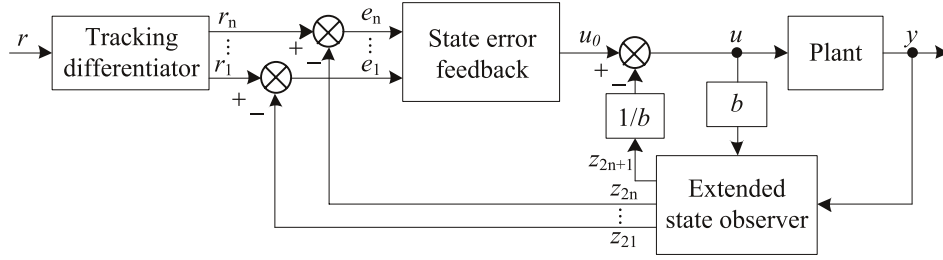


**Figure 2.** Control block diagram of active disturbance rejection controller.

#### 3.2.1. Speed Loop Active Disturbance Rejection Controller

The differential of motor speed is affected by  $i_d$ ,  $i_q$  and  $T_L$ , and the expression is

$$\frac{d\omega_e}{dt} = \frac{1}{J} [1.5n_p^2 (\lambda_f i_q + (L_d - L_q) i_d i_q) - n_p T_L - B\omega_e] \quad (6)$$

According to the principle of ADRC,  $\frac{1}{J}[1.5n_p^2(L_d - L_q)i_d i_q - n_p T_L - B\omega_e]$  in (6) is regarded as the disturbance  $f_w$  of the speed loop,  $i_q$  as the input  $u$ , and  $\frac{1.5n_p^2 \lambda_f}{J}$  as the coefficient  $b$ . From the ADRC observation of the perturbation  $f_w$ , (6) can be redescribed as

$$\frac{d\omega_e}{dt} = \frac{1.5n_p^2 \lambda_f}{J} i_q + f_w = bu + f_w \quad (7)$$

The structure of the speed loop regulator constructed by ADRC is shown in Fig. 3. As can be seen from Fig. 3, the speed loop ADRC includes two links, linear ESO (LESO) and linear SEF (LSEF). ADRC uses LESO to estimate the controlled object. In this process, not only the estimated values of each state variable, but also the internal and external disturbance estimates can be obtained. The estimated disturbance can be used to compensate the LSEF control signal.

The LESO in Fig. 3 can be written as

$$\begin{cases} e_0 = z_{21} - \omega_e \\ \dot{z}_{21} = z_{22} - \beta_1 e + bu \\ \dot{z}_{22} = -\beta_2 e \end{cases} \quad (8)$$

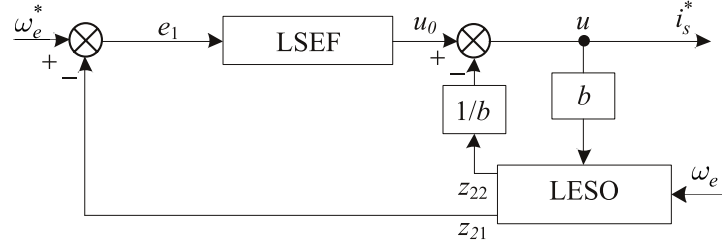


Figure 3. ADRC structure of speed loop.

where  $z_{21}$  is the speed observation value;  $z_{22}$  is the disturbance observation value; and  $\beta_1$  and  $\beta_2$  are the observer gains.

LSEF can be written as

$$\begin{cases} e_1 = \omega_e^* - z_{21} \\ u_0 = \beta_3 e_1 \end{cases} \quad (9)$$

where  $\beta_3$  is the controller gain.

The compensation output of disturbance is

$$u = u_0 - \frac{z_{22}}{b} \quad (10)$$

After the speed loop ADRC is designed, the same method can be used to design the current loop ADRC.

### 3.2.2. Current Loop Active Disturbance Rejection Controller

Convert (1) into current differential form, which can be expressed as

$$\begin{cases} \frac{di_d}{dt} = \frac{1}{L_d} (u_d - R_s i_d + \omega L_q i_q) \\ \frac{di_q}{dt} = \frac{1}{L_q} (u_q - R_s i_q - \omega L_d i_d - \omega \lambda_f) \end{cases} \quad (11)$$

Take the stator voltage  $u_d$  and  $u_q$  as the input  $\mathbf{u}_c$ ,  $1/L_s$  is  $b_c$ , and  $(-R_s i_d + \omega L_q i_q)/L_d$  and  $(-R_s i_q - \omega L_d i_d - \omega \lambda_f)/L_q$  are regarded as disturbance  $\mathbf{f}_c$ . (11) is rewritten into matrix form

$$\begin{bmatrix} \dot{i}_d \\ \dot{i}_q \end{bmatrix} = \frac{1}{L_s} \begin{bmatrix} u_d \\ u_q \end{bmatrix} + \begin{bmatrix} f_{c1} \\ f_{c2} \end{bmatrix} \quad (12)$$

$$\mathbf{i}_s = b_c \mathbf{u}_c + \mathbf{f}_c \quad (13)$$

where  $\mathbf{i}_s = [i_d \ i_q]^T$ ,  $\mathbf{u}_c = [u_d \ u_q]^T$ ,  $\mathbf{f}_c = [(-R_s i_d + \omega L_q i_q)/L_d \ (-R_s i_q - \omega L_d i_d - \omega \lambda_f)/L_q]^T$ .

(12) also conforms to the construction paradigm of ADRC, so it can also be designed as an ADRC. The current loop ADRC control structure is shown in Fig. 4. As can be seen from Fig. 4, the current loop ADRC is also composed of LESO and LSEF. Its basic structure is consistent with (8)–(10).

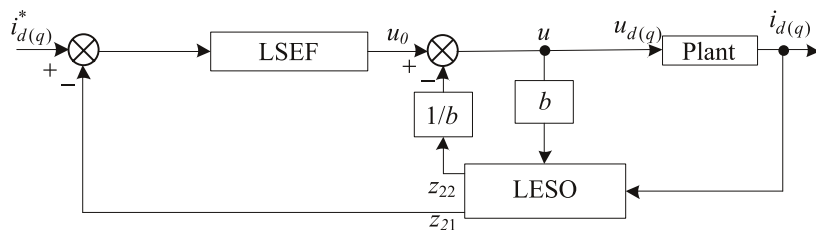


Figure 4. ADRC structure of current loop.

### 3.3. Parameter and Stability Analysis

The ADRC in speed loop and current loop is a first-order ADRC structure. In order to analyze its stability, firstly, the state space equation is constructed

$$\begin{cases} \dot{\mathbf{x}} = \mathbf{A}\mathbf{x} + \mathbf{B}u + \mathbf{E}h \\ \mathbf{y} = \mathbf{C}\mathbf{x} \end{cases} \quad (14)$$

where  $\mathbf{A} = \begin{bmatrix} 0 & 1 \\ 0 & 0 \end{bmatrix}$ ,  $\mathbf{B} = \begin{bmatrix} b \\ 0 \end{bmatrix}$ ,  $\mathbf{C} = [1 \ 0]$ ,  $\mathbf{E} = \begin{bmatrix} 0 \\ 1 \end{bmatrix}$ .

The corresponding LESO is

$$\begin{cases} \dot{\mathbf{z}} = \mathbf{A}\mathbf{z} + \mathbf{B}u + \mathbf{L}(y - \hat{y}) \\ \hat{\mathbf{y}} = \mathbf{C}\mathbf{z} \end{cases} \quad (15)$$

where  $\mathbf{L}$  is the observer gain,  $\mathbf{L} = [\beta_1 \ \beta_2]^T$ .

By configuring  $\mathbf{L}$ , the observation system can be stable, and different gain coefficients will make the system show different control performances.

In order to prove the stability of the observation system, subtract (15) from (14) to obtain

$$\begin{aligned} \dot{\mathbf{x}} - \dot{\mathbf{z}} &= \mathbf{A}\mathbf{x} + \mathbf{B}u - \mathbf{A}\mathbf{z} - \mathbf{B}u - \mathbf{L}(y - \hat{y}) \\ &= \mathbf{A}(\mathbf{x} - \mathbf{z}) - \mathbf{L}(\mathbf{C}\mathbf{x} - \mathbf{C}\mathbf{z}) \\ &= (\mathbf{A} - \mathbf{L}\mathbf{C})(\mathbf{x} - \mathbf{z}) \end{aligned} \quad (16)$$

Taking  $(\mathbf{x} - \mathbf{z})$  as the error and recording as  $\mathbf{e}_s$ , the error matrix can be transformed into

$$\dot{\mathbf{e}}_s = (\mathbf{A} - \mathbf{L}\mathbf{C})\mathbf{e}_s = \mathbf{H}\mathbf{e}_s \quad (17)$$

The eigenvalue of  $\mathbf{H}$  determines the control performance of the system. Therefore, the reasonable design of the eigenvalue of  $\mathbf{H}$  can ensure the stability of the system. Its characteristic equation is

$$|\lambda\mathbf{I} - (\mathbf{A} - \mathbf{L}\mathbf{C})| = 0 \quad (18)$$

where  $\mathbf{I}$  is the unit matrix.

After expanding (18), the following formula can be obtained

$$\lambda^2 + \beta_1\lambda + \beta_2 = 0 \quad (19)$$

where  $\lambda$  is the characteristic value of  $\mathbf{H}$ , and  $\beta_1$  and  $\beta_2$  are the observer gains.

In order to associate the control system parameters with the bandwidth, let the eigenvalue  $\lambda_1 = \lambda_2 = -\omega_0$ , so (19) can be rewritten as

$$\omega_0^2 - \beta_1\omega_0 + \beta_2 = 0 \quad (20)$$

Here, taking  $\beta_1 = 2\omega_0$  and  $\beta_2 = \omega_0^2$ , (20) can be established. Therefore, the gain matrix  $\mathbf{L} = [2\omega_0 \ \omega_0^2]^T$ .

When the gain matrix  $\mathbf{L} = [2\omega_0 \ \omega_0^2]^T$ , the error matrix corresponding to (17) will approach 0, and the whole observer system will remain stable.

### 3.4. Total Control System Design

This article uses the speed loop ADRC and current loop ADRC to control the FW control system. The overall control block diagram is shown in Fig. 5. During the entire control process, the speed loop ADRC is used to adjust the motor speed. According to the design in Section 3.3, different control effects are achieved by configuring different bandwidths. The current vector command output by the speed loop ADRC is used as the input signal of the leading angle FW control algorithm. In the leading angle FW control algorithm, the integral operation is performed according to the difference between the voltage vector and the maximum voltage value; the operation structure is taken as the leading angle; and the  $d$ - $q$  axis currents are adjusted. The leading angle FW control is to use the output  $d$ - $q$  axis currents as the input signals of the current loop ADRC, and also use the gain coefficient designed in Section 3.3 to adjust the control system. It should be noted that the bandwidth of the current loop is generally higher than that of the speed loop; therefore, the gain of the current loop observer needs to be set larger in the actual adjustment process.

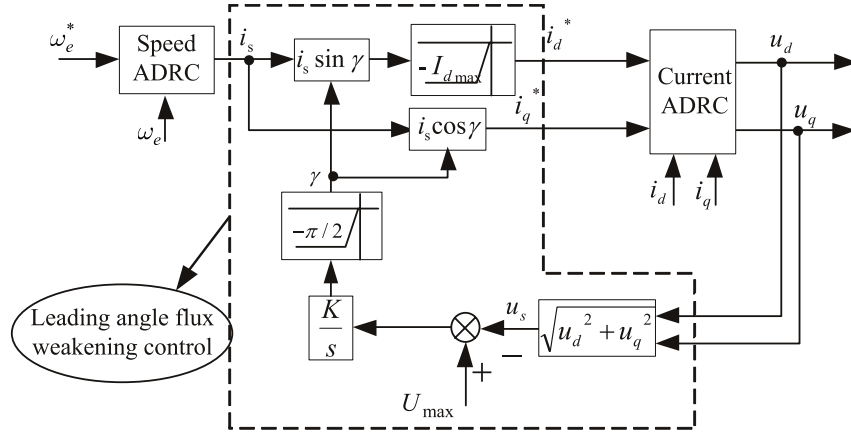


Figure 5. Overall control block diagram.

4. EXPERIMENT AND ANALYSIS

In order to verify the control effect of the proposed method, the experiments of FW control based on ADRC leading angle are carried out on the experimental platform shown in Fig. 6. In the experimental platform, TMS320F28335 of Texas Instruments is used as the control unit, and intelligent power module of Mitsubishi is used as the driving module. The basic parameters of the experimental motor are shown in Table 1. Due to the limitation of the mechanical structure of the encoder, the experimental speed is 6500 r/min, and the given load is 0.2 N·m. The proposed method is compared with the PI controller method. Between them, the parameters of speed loop PI controller in PI controller method are  $k_p = 2e - 2$ ,  $k_i = 5e - 5$ . The PI controller parameters of  $d$ - $q$  axis current loop are  $k_p = 8$ ,  $k_i = 8e - 2$ . In the ADRC leading angle FW control method, the parameters of speed loop LSEF are  $\beta_3 = 2e - 2$ ,  $b = 7277$ , and the observer bandwidth of LESO is  $\omega_{0s} = 300$ . The parameters of LSEF of current loop  $\beta_3 = 8$ ,  $b = 200$ , and the observer bandwidth of LESO is  $\omega_{0i} = 600$ . The integral coefficient of two

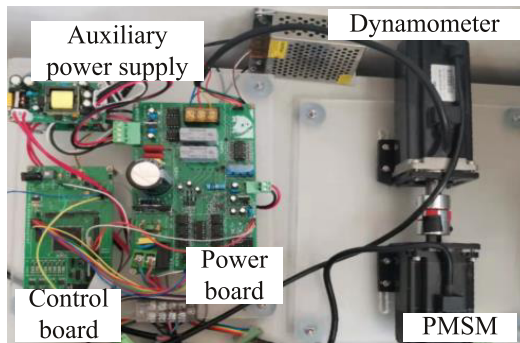
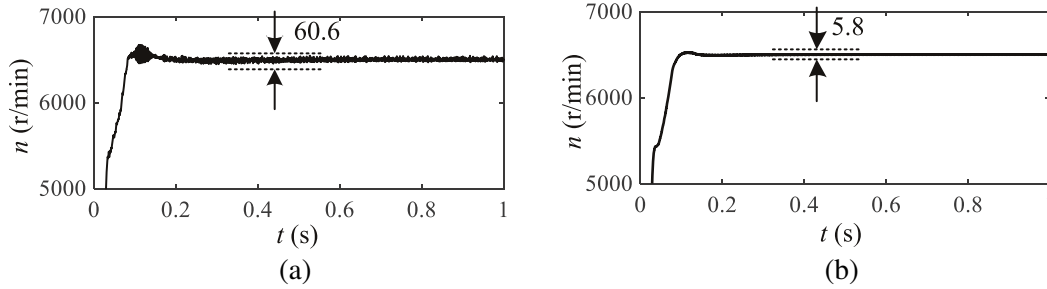


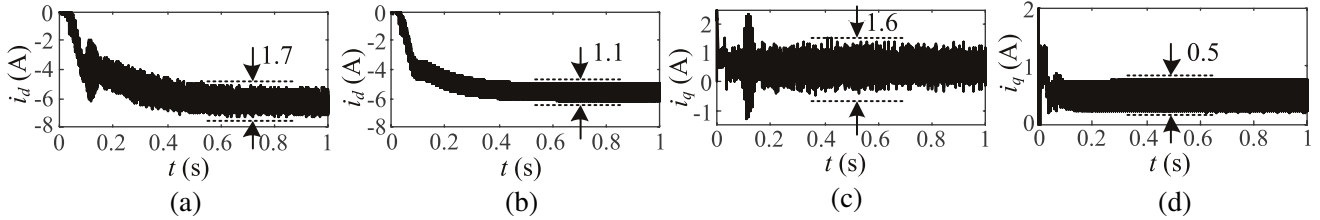
Figure 6. Schematic diagram of the experimental platform.

Table 1. Parameters of the prototype.

Parameters	Value	Parameters	Value
Stator resistance $R$ ( $\Omega$ ) and inductance $L_s$ (H)	1.6/0.005075	Rated power $P$ (kW)	0.2
Pole Pairs	4	Rated voltage $U$ (V)	220
Permanent magnet flux $\lambda_f$ (Wb)	0.0825	Rated current $I$ (A)	2.1
Rated speed $n_N$ (r/min)	3000	Rated torque $T_e$ (N·m)	0.64



**Figure 7.** Speed waveforms. (a) PI method. (b) Proposed method.



**Figure 8.** Current waveforms. (a)  $d$ -axis, PI method. (b)  $d$ -axis, proposed method. (c)  $q$ -axis, PI method. (d)  $q$ -axis, proposed method.

kinds of leading angle FW control is  $2e - 3$ .

Figures 7(a)–(b) are waveforms of the rotational speed using the PI control method and the proposed control method. As can be seen from Fig. 7, both control methods can make the motor run stably at a given speed. However, the PI control method has greater jitter during the dynamic adjustment process, and in the steady-state operation, the speed fluctuation is 60.6 r/min, while the speed fluctuation of the proposed method is only 5.8 r/min. Compared with PI control method, the speed fluctuation of the proposed method is reduced by 90.43%.

Figures 8(a)–(d) are the  $d$ - $q$  axis current waveforms of two control methods. Fig. 8(a) and Fig. 8(b) are the  $d$ -axis current waveforms, and Fig. 8(c) and Fig. 8(d) are the  $q$ -axis current waveforms. As can be seen from Fig. 8, when the motor is in steady state, the  $d$ - $q$  axis currents jitter amplitudes of PI control method are 1.7 A and 1.6 A, respectively, while the  $d$ - $q$  axis currents jitter amplitudes of the proposed method are 1.1 A and 0.5 A, respectively. Compared with PI control method, the amplitudes of  $d$ - $q$  axis currents jitter of the proposed method are reduced by 35.29% and 68.75%, respectively.

Figures 9(a)–(b) are torque waveforms of two control methods. As can be seen from Fig. 9, when the motor is in steady state, the torque fluctuation of PI control method is 0.6 N·m, while the torque fluctuation of the proposed control method is only 0.2 N·m. Compared with the PI control method, the torque jitter amplitude of the proposed method is reduced by 66.67%.

Figures 10(a)–(b) are the speed waveforms of the two control methods when the load changes

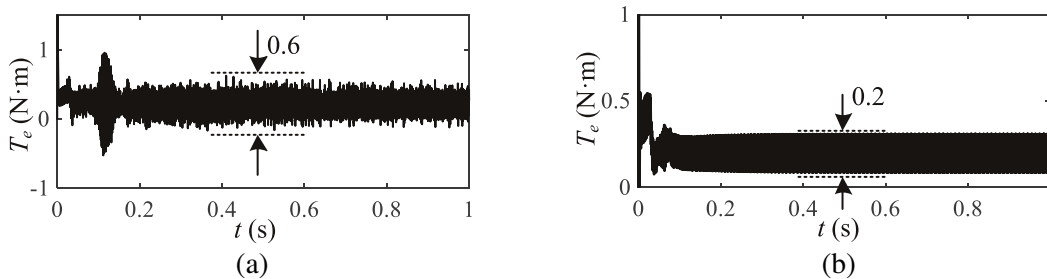


**Figure 9.** Torque waveforms. (a) PI method. (b) Proposed method.

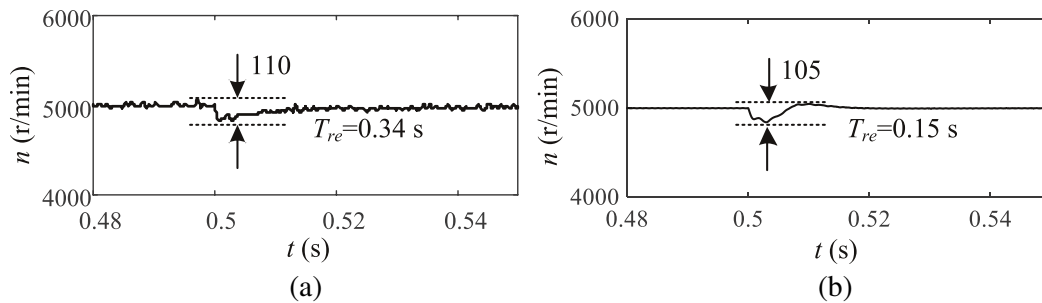


**Figure 10.** Speed waveforms. (a) PI method. (b) Proposed method.

suddenly. At 0.5s, the load changes from 0.2N·m to 0.6N·m. Due to flux weakening control, the given speed is adjusted to 5000 r/min; otherwise the speed will not reach the given value due to power limitation. At this time, when the load torque changes abruptly, the speed change of the two control methods is basically suppressed, but the recovery time  $T_{re}$  of the proposed method is 0.15s, while the recovery time  $T_{re}$  of the PI control method is 0.34s, so the proposed method has better dynamic performance.

In conclusion, the proposed method not only has better control effect in dynamic control, but also has better disturbance suppression ability in steady-state operation.

## 5. CONCLUSION

Since the parameters of PI controllers cannot be applied to the entire operating range of the motor speed control process, a leading angle FW control method based on active disturbance rejection method is proposed to improve the control performance of motor at high speed. The experimental results show that when the motor is in a steady state, the amplitudes of the speed fluctuation, stator current fluctuation, and torque fluctuation of the proposed control method are smaller than those of the PI control method. The parameter adjustment of the proposed ADRC method is directly related to the bandwidth, which makes the motor parameter adjustment process more convenient and provides a reference for practical applications.

## REFERENCES

1. Liu, X., Y. Pan, Y. Zhu, H. Han, and L. Ji, "Decoupling control of permanent magnet synchronous motor based on parameter identification of fuzzy least square method," *Progress In Electromagnetics Research M*, Vol. 103, 49–60, 2021.
2. Zhu, Y., Y. Bai, H. Wang, and L. Sun, "Sensorless control of permanent magnet synchronous motor based on T-S fuzzy inference algorithm fractional order sliding mode," *Progress In Electromagnetics Research M*, Vol. 105, 161–172, 2021.
3. Miguel-Espinar, C., D. Heredero-Peris, G. Gross, M. Llonch-Masachs, and D. Montesinos-Miracle, "Maximum torque per voltage flux-weakening strategy with speed limiter for PMSM drives," *IEEE Transactions on Industrial Electronics*, Vol. 68, No. 10, 9254–9264, Oct. 2021.
4. Zhang, Z., C. Wang, M. Zhou, and X. You, "Flux-weakening in PMSM drives: Analysis of voltage angle control and the single current controller design," *IEEE Journal of Emerging and Selected Topics in Power Electronics*, Vol. 7, No. 1, 437–445, Mar. 2019.
5. Li, J., S. Ekanayake, M. F. Rahman, R. Dutta, X. Huang, J. Ma, and Y. Fang, "Deep flux weakening control with six-step overmodulation for a segmented interior permanent magnet synchronous motor," *2017 20th International Conference on Electrical Machines and Systems (ICEMS)*, 1–6, Aug. 2017.

6. Liu, Q. and K. Hameyer, "A deep field weakening control for the PMSM applying a modified overmodulation strategy," *8th IET International Conference on Power Electronics, Machines and Drives (PEMD)*, 1–6, Apr. 2016.
7. Wang, H., T. Wang, X. Zhang, and L. Guo, "Voltage feedback based flux-weakening control of IPMSM with fuzzy-pi controller," *International Journal of Applied Electromagnetics and Mechanics*, Vol. 62, No. 1, 31–43, Jan. 2019.
8. Ding, D., G. Wang, N. Zhao, G. Zhang, and D. Xu, "Enhanced flux-weakening control method for reduced DC-link capacitance ipmsm drives," *IEEE Transactions on Power Electronics*, Vol. 34, No. 8, 7788–7799, Aug. 2019.
9. Deng, T., Z. Su, J. Li, P. Tang, X. Chen, and P. Liu, "Advanced angle field weakening control strategy of permanent magnet synchronous motor," *IEEE Transactions on Vehicular Technology*, Vol. 68, No. 4, 3424–3435, Apr. 2019.
10. Zhou, K., M. Ai, D. Sun, N. Jin, and X. Wu, "Field weakening operation control strategies of PMSM based on feedback linearization," *Energies*, Vol. 12, No. 23, 4526, Nov. 2019.
11. Trancho, E., E. Ibarra, A. Arias, I. Kortabarria, J. Jurgens, L. Marengo, A. Fricassè, and J. V. Gragger, "PM-assisted synchronous reluctance machine flux weakening control for EV and HEV applications," *IEEE Transactions on Industrial Electronics*, Vol. 65, No. 4, 2986–2995, Apr. 2018.
12. Jin, X., Y. Zeng, and D. Xu, "Novel PMSM field-weakening control method," *IECON*, 3744–3748, Oct. 2017.
13. Ekanayake, S., R. Dutta, and M. F. Rahman, "A modified single-current-regulator control scheme for deep flux-weakening operation of interior permanent magnet synchronous motors," *The Annual Conference of the IEEE Industrial Electronics Society*, 2624–2629, 2016.
14. Zhang, X., Z. Zhao, and C. Xu, "A flux-weakening method for pmsm based model predictive direct speed control," *2020 IEEE 9th International Power Electronics and Motion Control Conference (IPEMC2020-ECCE Asia)*, 2557–2561, Nov. 2020.
15. Liu, J., C. Gong, Z. Han, and H. Yu, "IPMSM model predictive control in flux-weakening operation using an improved algorithm," *IEEE Transactions on Industrial Electronics*, Vol. 65, No. 12, 9378–9387, Dec. 2018.
16. Qu, L., W. Qiao, and L. Qu, "An enhanced linear active disturbance rejection rotor position sensorless control for permanent magnet synchronous motors," *IEEE Transactions on Power Electronics*, Vol. 35, No. 6, 6175–6184, Jun. 2020.
17. Zuo, Y., X. Zhu, L. Quan, C. Zhang, Y. Du, and Z. Xiang, "Active disturbance rejection controller for speed control of electrical drives using phase-locking loop observer," *IEEE Transactions on Industrial Electronics*, Vol. 66, No. 3, 1748–1759, Mar. 2019.